Materials & Design 234 (2023) 112359

Contents lists available at ScienceDirect

Materials & Design

journal homepage: www.elsevier.com/locate/matdes

Microstructural and micromechanical property characterisation of CF/PEKK composites using nanoindentation

Helena Pérez-Martín [a], Paul Mackenzie [b], Alex Baidak [b], Conchúr M. Ó Brádaigh [a], Dipa Ray [a,*]

[a] School of Engineering, Institute for Materials and Processes, The University of Edinburgh, Edinburgh, United Kingdom
[b] Hexcel Composites Ltd., Duxford, Cambridge, United Kingdom

ARTICLE INFO

Keywords:
CF/PEKK
Composite
Automated tape placement
Nanoindentation
Thermoplastic matrix
Interphase

ABSTRACT

The present work seeks to characterise the micromechanical properties of carbon fibre/poly(etherketoneketone) (CF/PEKK) composites with different crystallinity levels and morphologies. CF/PEKK laminates were manufactured under various compression-moulding and automated tape placement (ATP) conditions. Nanoindentation experiments were performed at different locations across the thickness of the laminates to evaluate hardness and elastic modulus at the micron scale. The polymer matrix of compression-moulded laminates, which was found to be fully crystallised, performed significantly better than the matrix of the ATP laminates. The central region of the ATP laminates performed slightly better than regions close to the top and bottom surfaces, likely due to a higher crystallisation development in the central area. A transition in response from the fibre to the matrix bulk was observed across all samples via nanoindentation testing. Overall, the study of micromechanical properties can provide insight into the impact of manufacturing conditions on the composite's performance at the macro scale, ultimately contributing towards higher-quality end products. To the authors' best knowledge, the in-depth work presented in this article is the first to use nanoindentation to characterise the effect of manufacturing processes on the micromechanical properties of CF/PEKK laminates.

1. Introduction

Poly(aryletherketones) (PAEKs) are a family of semicrystalline thermoplastics of high interest as a polymer matrix in composites, due to their suitability for high-performance applications. Poly(ether-etherketone) (PEEK), the most established of this polymer family, has been widely studied and is currently a popular option for advanced composites [1,2]. In recent years, poly(etherketoneketone) (PEKK) is also becoming an increasingly attractive choice due to the tuneability of the molecule's backbone chain, allowing control of material density, crystallisation rate and resulting properties [3–5]. Studies have characterised crystallisation kinetics of various grades of unreinforced PEKK and CF/PEKK [4–7], as well as the composite's mechanical performance when manufactured using various techniques [8].

In-situ manufacturing techniques are of interest as these are more energy and time efficient than other conventional processing methods, such as compression moulding and autoclaving. Automated tape placement (ATP) is one of such manufacturing methods, attractive due to its automation, part repeatability, potential as a single-step process and lower waste production. In-situ manufacturing processes such as ATP, however, can compromise part quality due to very short exposure times to heat and pressure, resulting in limited consolidation and non-uniform crystallinity development. Published studies on in-situ manufacturing of CF/PEEK demonstrate that ATP can achieve properties close to autoclave values [9–12], however, in the case of CF/PEKK, whose crystallisation kinetics are slower, this needs further research [13].

The fast nature of ATP manufacturing also leads to uncertainties in the crystallinity evolution when the part is manufactured, as the already laid material sees heat repasses as more material is laid on top. At the same time, the tool upon which the material is laid can act as a heat sink if kept unheated; whereas, if heated, can cause void rebound within the part being manufactured when held above glass transition temperature after roller pressure is lost [14–16]. It is therefore essential to understand how processing conditions affect the final part's performance.

Work has been done on tracking the evolution of heat transfer [10,17] and its modelling [18–21], as well as some investigations on how this impacts crystallinity development [17,21]. The generation of uniform crystallinity throughout the bulk of a manufactured part is a key requirement for reliable performance during the service life. This is

* Corresponding author at: 1.140 Sanderson Building, King's Buildings, Edinburgh EH9 3FB, Scotland, United Kingdom.
E-mail address: Dipa.Roy@ed.ac.uk (D. Ray).

https://doi.org/10.1016/j.matdes.2023.112359
Received 17 July 2023; Received in revised form 13 September 2023; Accepted 24 September 2023
Available online 25 September 2023

quite challenging to achieve when a thermoplastic part is manufactured using ATP. The measurement of crystallinity across the thickness of laminates can provide insight into the effectiveness of the manufacturing method and potential areas of improvement during the manufacturing process. Differential scanning calorimetry (DSC) has been used by many researchers to evaluate crystallinity and morphology of ATP samples [8,9,11,12,14,17], however, DSC provides an average value of the entire sample being assessed. Lamontia and Gruber [22] assessed crystallinity variation of a CF/PEKK ATP laminate by milling different layers of a sample and then performing DSC, however, this is a quite laborious and time-intensive process. A different way of indirectly evaluating through-thickness crystallinity requiring less sample preparation is via micromechanical property characterisation with nanoindentation.

Nanoindentation is a technique that can be used to measure elastic modulus and hardness at micron and nano scales, which can thereby infer crystallinity. A method most commonly used in the field of metals and ceramics, it is increasingly used on a variety of polymers to test local properties [23–26]. Recent studies on unreinforced semicrystalline thermoplastics have shown that nanoindentation can be used to indirectly measure crystallinity of a sample by measuring their micromechanical properties. Christöfl et al. [25] successfully measured the variation in elastic modulus across an injection-moulded polyoxymethylene sample cross-section as a consequence of crystallinity and morphology variation. Indentations close to the sample surface displayed a lower elastic modulus than indentations in the bulk, due to top and bottom surfaces being in contact with injection-moulding tooling and cooling at a faster rate during manufacturing, therefore having a lower crystallinity. Similar behaviour has been observed in unreinforced PEEK [24,26,27], where a higher crystallinity resulted in increased hardness and elastic modulus values. A bimodal behaviour in fully crystallised PEEK was reported by Iqbal et al. [24], which was initially associated with the semicrystalline nature of the material. However, the indentation depths (6 μm) and reported spherulitic sizes of PEEK spherulites (10–20 μm) most likely provided the homogenised properties of the polymer rather than the two different phases, due to the resulting indentation being too large (a triangle with sides of about 30 μm [26]) to distinguish between the phases within a spherulitic structure. Voyiadjis et al. [26] suggested that this bimodal behaviour could therefore be due to surface inhomogeneities and studied the importance of surface finish in tough polymers (specifically PEEK) for nanoindentation to obtain consistent results. To the knowledge of the authors, no nanoindentation testing on unreinforced PEKK has been published.

The use of nanoindentation to characterise composite materials has risen since the 2000 s, with research characterising the reinforcement and matrix constituents of composites. The performance of the polymer matrix during nanoindentation experiments is influenced by the presence of fibres, particularly at large penetration depths [28], and polymer hardness and elastic modulus values are generally greater as a matrix in a composite than in neat form [29,30]. Nanoindentation has also been used to assess reinforcement-matrix interface and interphase properties. Interface generally refers to interfacial shear strength between fibre and matrix, where nanoindentation is used for fibre push-in testing; whereas interphase refers to a “third” transition phase between the fibre and matrix, tested via grid nanoindentation. Gibson [29] provides a review of work done on interfaces and interphases for a variety of polymer composites.

Nanoindentation has been used in the more recent years to characterise CF/PEEK ATP-manufactured laminates, some examples being as follows. Ray et al. [28] performed nanoindentation on CF/PEEK autoclaved and ATP laminates, corroborating previous findings that the presence of crystallinity results in a performance increase. Molazemhosseini et al. [31] studied PEEK-based composites with short CFs and nano-silica, successfully characterising fibre, matrix and interphase performance, as well as demonstrating an improvement in the performance of PEEK composites compared to its unreinforced form. Gain et al. [32] performed a study where the impact of consolidation force and hot gas torch temperature on the matrix and interphase properties were assessed, finding that increasing both parameters resulted in hardness and elastic modulus increases during nanoindentation testing. Additionally, nanoindentation has been used to evaluate the effect of ion irradiation on the micromechanical properties of unreinforced PEKK, [33] as well as its thermal degradation behaviour as a consequence of laser heating [34].

Nano-indentation research on CF/PEKK, on the other hand, is more limited, with no literature available on ATP-manufactured CF/PEKK composites. Gaillard and Amiot [35] performed nanoindentation testing on CF/PEKK prepreg tape in an attempt to observe and model the presence of an interphase with very low maximum loads of 60μN (and therefore very small indentations), achieving a very high spatial resolution. The matrix regions close to the fibre were found to be affected by the presence of the fibre, presenting a fibre-to-matrix modulus gradient ring around the fibre of approximately 800 nm thickness. It is important to keep in mind, however, that very small indentations (<50 nm depth) may produce unreliable results that are influenced by tip blunting or surface roughness [36]. Ramaswamy et al. [37] employed a nanoindenter to characterise fibre/matrix interfacial shear strength via fibre-pushout tests on autoclave-manufactured CF/PEKK laminates. Any further nanoindentation studies on crystallinity, the effects of varying parameters in a manufacturing process, or interphase characterisation of CF/PEKK have not been found by the authors of this work.

This work evaluates micromechanical properties of CF/PEKK laminates manufactured via compression moulding and ATP using nanoindentation, in order to indirectly measure crystallinity development and variation. DSC is initially used to assess the average crystallinity developed in each laminate as a consequence of the processing conditions. The impact of varying manufacturing parameters on the micromechanical properties is then studied via nanoindentation, as well as any variation in properties across the thickness of the ATP laminates. Additionally, the presence of any fibre/matrix property transition is evaluated.

2. Materials and methods

2.1. Materials

In this study, samples were manufactured with AS7 CF/PEKK unidirectional prepreg tape, provided by Hexcel Composites Ltd. The PEKK matrix was KEPSTAN PEKK 7002PT by Arkema. The tape for the compression-moulded laminates was 150 mm wide and had an average fibre volume fraction of 60.6 % (measured via acid digestion). The tape for the ATP laminates was 6.4 mm wide and had an average fibre volume fraction of 58.4 %. Both tapes had an average thickness of 0.2 mm.

2.2. Compression moulding manufacturing

Unidirectional compression-moulded laminates were manufactured using a 3-part mould (a 2 mm-thick frame with top and bottom plates). 10 sheets of prepreg tape were stacked and placed in the mould. A Pinette Emidecau Industries (PEI) LAB 450P hydraulic press was used, with a Frigosystem chiller providing the cooling.

A total of three laminates were manufactured with dimensions 300 mm × 150 mm × 2 mm, undergoing the following cycle:

1. Heat up from 20 °C to 370 °C at 10 °C/min.
2. Hold at 370 °C for 25 min.
3. Cool down from 370 °C to isothermal temperature (220 °C, 260 °C or 300 °C) at 10 °C/min.
4. Hold at isothermal temperature for 60 min.
5. Cool down from isothermal temperature to 20 °C at 10 °C/min.

The isothermal temperatures were selected based on a previous study on the crystallisation behaviour and morphology of PEKK and CF/PEKK composites [7]. The holding temperature in the melt of 370 °C is above the polymer's melting temperature (338 °C), and therefore ensures the removal of the matrix's thermal history. All laminates underwent a platen pressure of 1 bar during step 1, and 28 bar for the remaining steps.

A temperature–time plot of the above cycles is shown in Fig. 1. The laminate code denotes the processing condition ("CM" for compression moulding) and the isothermal hold temperature (220 °C, 260 °C or 300 °C).

2.3. Automated tape placement manufacturing

Unidirectional ATP laminates were manufactured using a laser-assisted tape placement head (AFPT, GmbH) attached to a robot arm (Kuka, KR240 L210-2). A total of 10 layers of prepreg tape were placed per laminate, with a laser repass performed on the final layer of each laminate. A diagram of the process and a summary of the ATP settings is shown in Fig. 2.

Three laminates with dimensions 300 mm × 150 mm × 2 mm were manufactured on a metallic tool, with a nip temperature (T_{nip}) of 380 °C, laydown speed of 2 or 4 m/min, roller pressure of 2 or 4 bar, and a laminate thickness of 2 mm.

Additionally, a multi-thickness laminate was manufactured on a ceramic tool, with a T_{nip} = 360 °C, lay-down speed of 4 mm/min, roller pressure of 2 bar. A section of this laminate was 2 mm thick (10 layers), and another 6 mm-thick (30 layers). A schematic of this laminate is shown in Fig. 3.

The laminate codes are given in Table 1. These denote the processing condition (ATP), T_{nip} (360 or 380 °C), lay-down speed (2 or 4 m/min) and roller pressure (2 or 4 bar). In the case of the 360 °C laminates, the code also includes the laminate thickness (2 or 6 mm). Comparisons of laminate properties and performance have been drawn across these three parameters in Section 3.

While recording the thermal history that the tape undergoes during lay-down was not possible during manufacturing, literature [17] has reported steep temperature drops during ATP manufacturing of CF/PEKK laminates on a cold tool, reaching cooling rates of 150–220 °C/min during the first seconds of cooling. These were observed to be higher on the first layers of prepreg tape laid on an unheated tool, likely due to the tool acting as a heat sink and the progressively larger amount of material between the tool and the incoming tape holding on to the heat produced by the ATP laser.

2.4. Differential scanning calorimetry (DSC)

Crystallinity measurements of the ATP samples with T_{nip} = 360 °C were carried out with a PerkinElmer DSC 8000. For the rest of the samples, this was done with a Mettler Toledo DSC 3+. In both instances, DSC scans from room temperature to 370 °C at 20 °C/min were run with non-hermetically sealed aluminium pans and lids under a nitrogen environment. Indium was used to calibrate the temperature and heat of fusion prior to any experiments. All samples weighed 8–20 mg. These were performed to evaluate the average crystallinity across the entire thickness of the manufactured laminates.

The crystallinity of a sample was calculated using:

$$\chi = \frac{\Delta H_m - \Delta H_{cc}}{\alpha \times \Delta H_{100\%}} \quad (1)$$

where ΔH_m is the melting enthalpy, ΔH_{cc} is the cold crystallisation enthalpy, α is the matrix weight fraction (31.7 % for the compression moulding tape and 34.5 % for the ATP tape, both measured via acid digestion) and $\Delta H_{100\%}$ is the theoretical melting enthalpy of 100 % crystalline PEKK. This has been calculated to be 130 J/g by Chang and Hsiao [38].

2.5. Nanoindentation

Samples measuring approximately 1 cm × 1 cm (2 mm thick) were cut out of the laminates with a hand saw and were mounted in epoxy resin, exposing the cross-section of the laminate. These were polished with silicon carbide discs of up to P2500, followed by diamond suspension polishing down to 1 μm particle size.

The nanoindentation tests were performed using a KLA iMicro Nanoindenter, with a diamond Berkovich-type indenter tip (ID: DC2/BERKOVICH/015). An initial calibration was performed with silica and glassy carbon to measure the frame stiffness and the area function of the tip.

Load-unload indentation cycles were performed using continuous stiffness measurement testing, at an indentation strain rate of 0.2 s^{-1}, a frequency of 110 Hz and frequency amplitude of 2 nm. Elastic modulus and hardness can be determined from the load–displacement curves obtained during testing, an example of which is shown in Fig. 4.

The contact stiffness S, which is the initial slope at the beginning of the unloading curve, can be expressed as defined by Pharr and Oliver

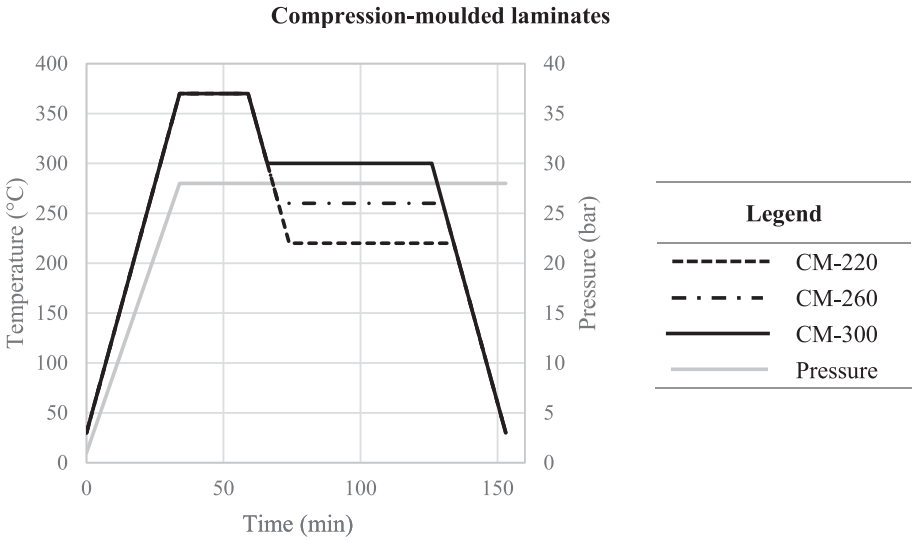

Fig. 1. Summary of processing parameters for the compression-moulded laminates.

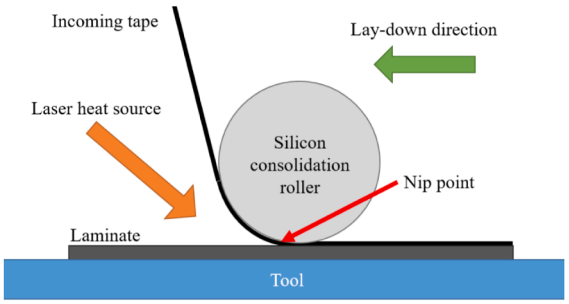

Cooler air pressure	1 bar
Incoming tape dimensions	6.4mm wide x 0.2mm thick
Laser-nip point optical distance	170mm
Laser power limit	1000W
Tape/laminate laser split	Approx. 50/50
Tool temperature	Unheated

Fig. 2. Schematic of ATP lay-up process and processing parameters.

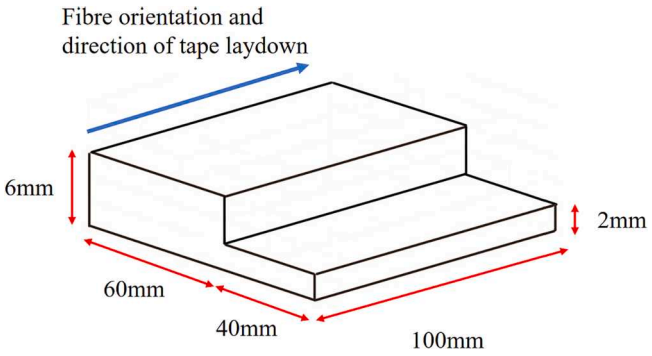

Fig. 3. Schematic of multi-thickness laminate, showing 2 mm and 6 mm thicknesses (not to scale).

Table 1
Summary of processing parameters for the ATP-manufactured laminates.

Laminate code	Tool material	Nip temperature (°C)	Lay-down speed (m/min)	Roller pressure (bar)	Laminate thickness (mm)
ATP-380-4-2	Mild steel	380	4	2	2
ATP-380-2-2	Mild steel	380	2	2	2
ATP-380-4-4	Mild steel	380	4	4	2
ATP-360-4-2-2 mm	Ceramic	360	4	4	2
ATP-360-4-2-6 mm	Ceramic	360	4	4	6

[39]:

$$S = \frac{2\beta}{\sqrt{\pi}} \times E_r \sqrt{A_c} \tag{2}$$

where E_r is the reduced elastic modulus and A_c is the indenter contact area (a function of the indenter depth in contact with the sample during testing). β is an indenter geometry constant introduced by Hay et al. [40] to account for different indenter tip geometries. E_r represents the elastic deformation that takes place in both the indenter and the sample, and is given by:

$$E_r = \left(\frac{1-\nu_i^2}{E_i} + \frac{1-\nu_s^2}{E_s} \right)^{-1} \tag{3}$$

where ν is Poisson's ratio, and the subscripts i and s denote the indenter and sample materials respectively. Assuming that $E_i \gg E_s$, the first term of Eq. (2) becomes negligible. Substituting Eq. (3) into Eq. (2) and rearranging,

$$E_s = \left(1-\nu_s^2\right) \times \frac{\sqrt{\pi}}{2\beta} \times \frac{S}{\sqrt{A_c}} \tag{4}$$

If the indenter is considered to be much stiffer than the sample, the sample hardness H can be defined by [41]:

$$H = \frac{P_{max}}{A_c} \tag{5}$$

where P_{max} is the maximum loading force achieved.

A 2 μm trial indentation in a matrix pocket, as shown in Fig. 5a, was performed to determine an adequate indentation depth. Fig. 5b shows that, above 1100 μm, there is a sharp increase in elastic modulus, indicating that fibres in the vicinity significantly influenced the matrix response at these depths. A lower depth is therefore preferable, in order to successfully evaluate the response of the composite's different constituents [29]. Based on this and previous work performed on CF/PEEK [26,28], a target indentation depth of 400 nm was chosen to take all elastic modulus and hardness values. In Fig. 5a, a 2 μm-deep indentation can be observed to be too large to do this in matrix areas closer to the fibre surface.

All samples were indented at locations marked with a square □ as shown in Fig. 6. At each location, a series of indentations were performed as given below:

- An array of nanoindentations to obtain hardness and elastic modulus values of the fibres and the matrix at different distances from the fibre surface, as shown with triangles Δ in Fig. 6;
- Two individual indents on matrix pockets to obtain matrix bulk properties, shown with stars ☆ in Fig. 6 (to ensure matrix bulk properties are characterised);
- Two individual indents on fibres to obtain fibre properties, as shown with crosses x in Fig. 6 (to ensure fibre properties are characterised).

A micrograph of an array and a matrix indent is shown in Fig. 8. The distance of the indentations to the closest fibre surface was measured using ImageJ software from the centre of the indentations to the surface of the nearest fibre edge.

The location and amount of nanoindentation arrays performed were chosen based on the expected crystallinity distribution across the thickness of the laminates. In the case of the compression-moulded laminates, crystallinity and morphology were assumed to be constant throughout the thickness due to the long holding times at crystallisation temperatures. Previous work done on these laminates [7] supported this assumption, showing homogeneous consolidation, high average crystallinity content and good mechanical performance. Therefore, a 5 × 5 array, two matrix indentations and two fibre indentations were performed at a single location (as shown in Fig. 6b) on compression-moulded samples, totalling 29 indentations per location □.

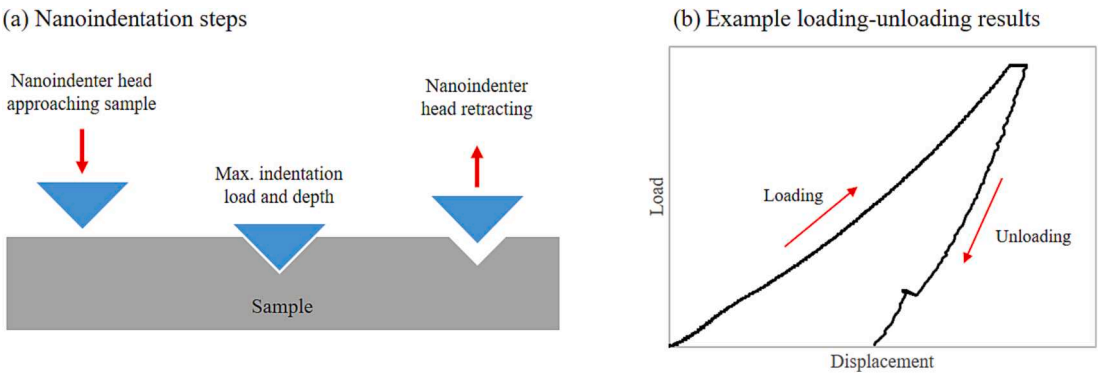

Fig. 4. (a) Nanoindentation loading and unloading schematic; and (b) sample load–displacement curve generated from a nanoindentation test.

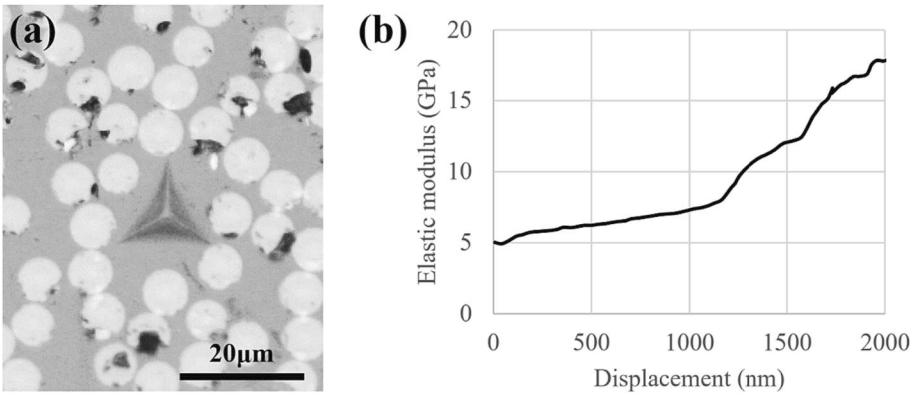

Fig. 5. (a) Micrograph of 2 μm depth indentation at a matrix pocket; and (b) elastic modulus-displacement plot of said indentation.

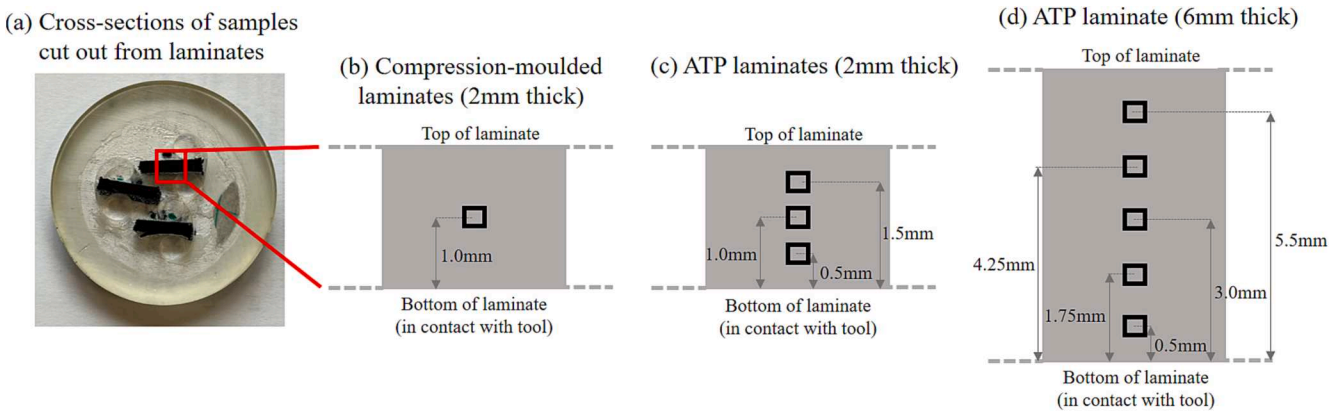

Fig. 6. Schematics of laminate cross-sections, showing the location of performed indentations with a square □.

On the other hand, the fast nature of ATP manufacturing is likely to result in a difference in crystallinity and morphology across the laminate thickness. This is supported by observations of poor laminate consolidation and low average crystallinity in our previous work [7], as well as a varying crystallinity content across the thickness of CF/PEEK and CF/PEKK ATP laminates as reported in literature [17,22]. Therefore, 3 × 5 arrays (plus two matrix and two fibre indentations) were performed at several locations across thicknesses of the ATP samples to assess this variation, resulting in 19 indentations per location □. For 2 mm-thick ATP laminates, 3 locations were tested (as shown in Fig. 6c); for the 6 mm-thick laminate, 5 locations were tested (as shown in Fig. 6d).

3. Results and discussion

3.1. Crystallinity content

Table 2 shows the total crystallinity achieved in the manufactured laminates. All compression-moulded laminates crystallised to the highest extent (~29 %), as expected due to the long holding times within crystallisation temperatures; whereas the ATP-manufactured laminates only achieved crystallinities up to 3–8 % overall. The marginally higher crystallinity of ATP-380-2-2 is likely due to the slower lay-down speed during manufacturing, keeping the material at temperatures which allow for crystallisation to take place for longer. Further discussion of the crystallinity content, morphology and DSC curves for the compression-moulded laminates and the ATP laminates with T_{nip} =

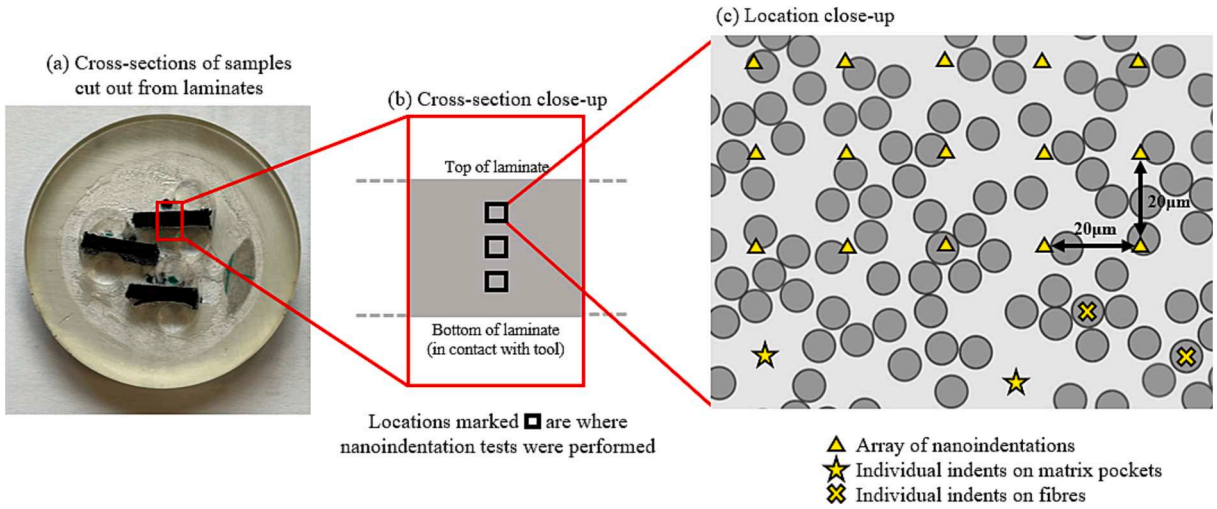

Fig. 7. Schematic example of an indentation array and fibre and matrix indents on an ATP sample. In this case, 19 indentations are being performed per location marked with a square □, with each of them giving hardness and elastic modulus data.

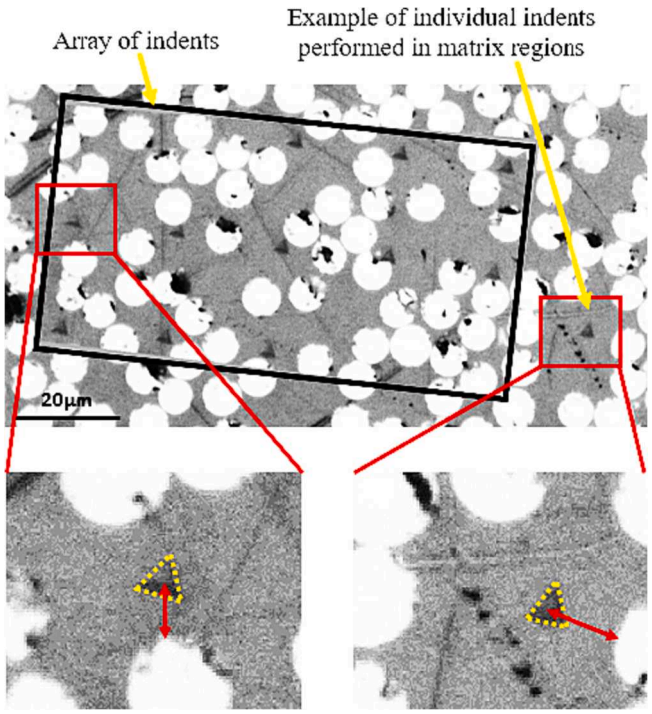

Fig. 8. A micrograph showing array and a matrix indent. A close-up of two indentations shows nanoindentation distances to the closest fibre surface marked with red arrows, measured using ImageJ. (For interpretation of the references to colour in this figure legend, the reader is referred to the web version of this article.)

380 °C can be found in our previous work [8], and a comprehensive study of crystallisation kinetics and modelling of the prepregs used in this work can be found in [7].

3.2. Nanoindentation

The following sections discuss the differences observed in load–displacement curves for compression-moulded and ATP laminates. This is followed by a brief explanation of the data processing procedure. Then matrix bulk properties are analysed and compared across different laminates and locations, as well as any variation in properties across the fibre/matrix interphase.

Table 2
Total crystallinity of CF/PEKK laminates manufactured under different processing conditions.

Laminate	Crystallinity (%)
CM-220	29.3 ± 1.4
CM-260	27.0 ± 1.0
CM-300	29.1 ± 1.3
ATP-380-4-2	6.8 ± 1.3
ATP-380-2-2	8.3 ± 1.0
ATP-380-4-4	6.0 ± 1.6
ATP-360-4-2-2 mm	3.4 ± 0.9
ATP-360-4-2-6 mm	4.6 ± 3.1

3.2.1. Load-displacement curves

Fig. 9a and b show load–displacement curves for all indentations done on sample CM-220 and the top location of ATP-380–4-2 respectively. These are provided as representative examples of the response of compression-moulded and ATP laminates, as this section draws a general comparison of the two manufacturing techniques, and not of the individual laminates. In these, as well as the rest of the nanoindentation results, three distinct responses can be observed, denoted as “fibre”, “matrix” and “interphase” in Fig. 9. Note that results obtained by indentations marked with a star ☆ in Fig. 7 fall in the matrix response, and results obtained by indentations marked with a cross x fall in the fibre response. Indentations marked with a triangle Δ may fall within any of these three categories, depending on where the indentation is made (on the fibre, in the matrix bulk, or in the matrix closer to a fibre surface).

The fibre response is the stiffest among all regions, experiencing the largest elastic recovery compared to matrix and interphase responses. This is observed in existing nanoindentation work on CF/PEEK [31]. While the fibres in all samples are identical, a lower peak load response in the ATP sample of 17-20mN can be observed, against 20-25mN of the compression-moulded sample. This may be due to the fibre behaving as part of a composite during nanoindentation rather than in isolation. Due to the elastic response of the fibre, no permanent dents were left after nanoindentation testing – this is visible in the nanoindentation array in Fig. 8, where permanent dents on matrix regions are visible but those that fell on fibres are not. Because of this, the indentation distance from the centre of the fibre could not be measured.

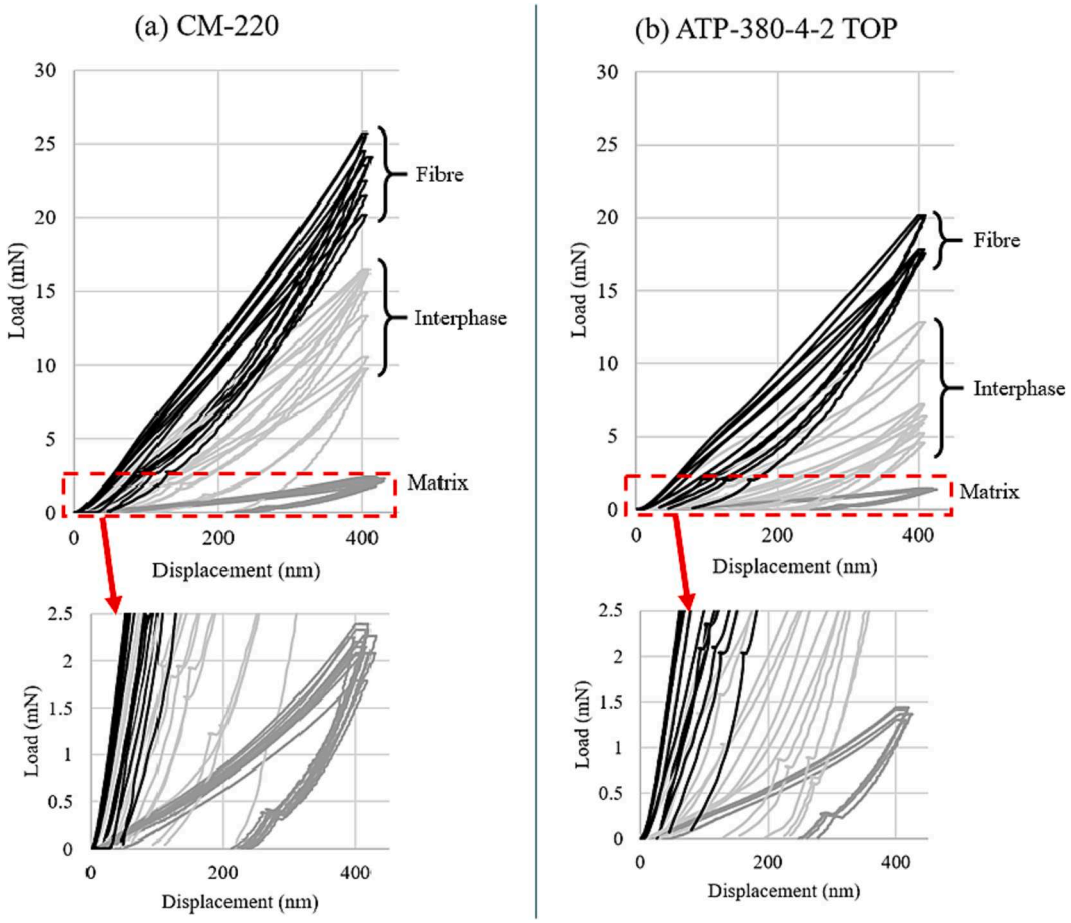

Fig. 9. Load-displacement results of nanoindentation experiments on (a) CM-220 and (b) the top location of ATP-380-4-2.

Matrix behaviour refers to the bulk response far away from any fibres, where performance remained similar across all load–displacement curves irrespective of the distance from fibre surfaces. An example location of this can be seen in Fig. 7 marked with stars ☆. A prominent hysteresis loop can be observed, related to the viscoelastic behaviour of PEKK. The compression-moulded sample withstood a higher load and experienced a smaller hysteresis loop. This is visible in the zoomed-in plots in Fig. 9a and b, where the indentation depth retained after the nanoindenter head is withdrawn ranges from 210 to 235 nm for the compression-moulded sample and 245–280 nm for the ATP sample (values read from the x-axes in Fig. 9). This can be attributed to the high crystallinity content in the compression-moulded samples resulting in a stiffer, more elastic response compared to that observed in the amorphous matrix of the ATP sample.

The interphase region refers to the response that does not match the fibre or matrix bulk response, but instead varies with the distance from the fibre surface at which the indentation was made. In the following section, it will be observed that nanoindentation tests closer to the fibre surface resulted in a stiffer response. The stiffer responses shown in Fig. 9 (higher loads at the same displacement) also possess smaller hysteresis loops, in line with the more elastic response as indentations are performed closer to fibre surfaces.

Similar observations have been made for a variety of polymers and polymer composites in literature. Molazemhosseini et al. [31] performed nanoindentation testing on short CF/PEEK samples (some reinforced with nano silica particles) and reported similar fibre/matrix/interphase responses as observed in this work. In their case, fibres exhibited perfect elastic response, likely due to the lower depth of indentations in all the testing (10–70 nm). Shen et al. [42] observed an increase in indentation resistance with a higher crystallinity content in unreinforced PA6, in a similar way to the stiffer performance of the more crystallised compression-moulded samples in this work. Klapperich et al. [23] tested a range of unreinforced PE grades with different molecular weights, and found those with lower crystallinity to exhibit a more pronounced hysteresis loop, and experience a significantly higher amount of deformation under the same load due to a more compliant response of the amorphous fraction in the sample.

3.2.2. *Hardness and elastic modulus against indentation distance from fibre surface: curve fitting*

The nanoindentation results for each location marked with a square □ in Fig. 6 provided hardness and elastic modulus data, which were plotted against the distance from the fibre surface at which each data point was taken. An example of this is given in Fig. 10, where hardness and elastic modulus results for the single location in laminate CM-260 are plotted. These results show a plateau far away from the fibre surface. For results analysis and comparative purposes, an exponential decay function was fitted to the results of each location. Examples of these are shown with the dotted curves in Fig. 10.

The exponential decay equation in question has the following form:

$$y = Aexp(-Bx) + C \tag{6}$$

where x is the distance from the fibre surface (μm), y is fibre hardness (or elastic modulus) (GPa), and A, B and C are constants. The number of constants to be found can be reduced by introducing the following boundary conditions:

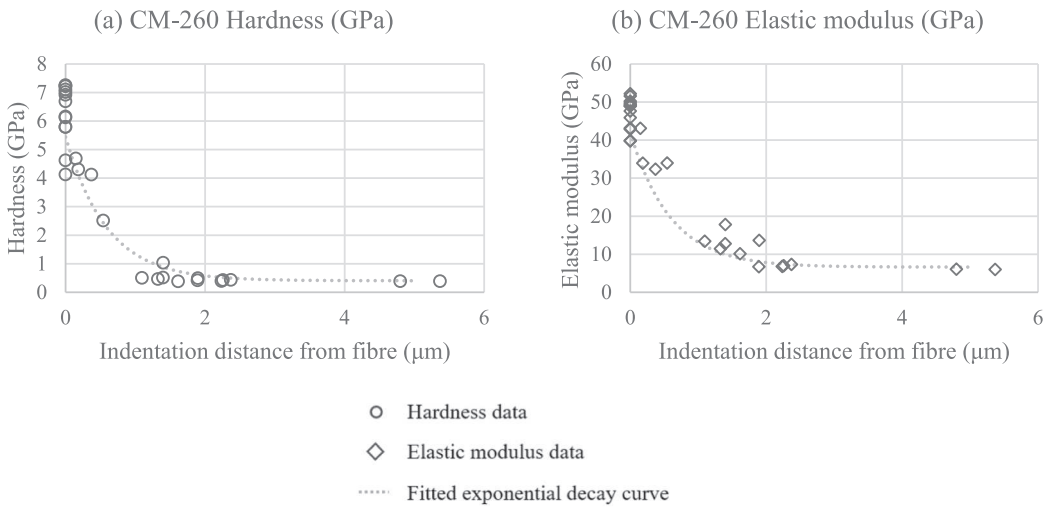

Fig. 10. (a) Hardness and (b) elastic modulus results against indentation distance from fibre surface for CM-260. The experimental data includes the nanoindentation array and individual indents performed on matrix pockets and fibres. The curves are fitted to the experimental data, and correspond to Eq. (9) and (10) for (a) and (b) respectively.

- When $x = 0$, $y = H_F$ (or M_F), the fibre hardness (or fibre elastic modulus). This value remains the same across all locations, as they all use the same fibre type. Substituting and rearranging:

$$y = Aexp(-Bx) + H_F - A \tag{7}$$

$$y = Aexp(-Bx) + M_F - A \tag{8}$$

- When $x = \infty$, $y = H_M$ (or M_M), the matrix hardness (or matrix elastic modulus). This value changes with each location, now that the processing conditions will affect the matrix morphology and crystallinity, and therefore its properties. This includes different locations within the same sample, as is the case with ATP samples. Substituting and rearranging:

$$y = (H_F - H_M)\exp(-B_H x) + H_M \tag{9}$$

$$y = (M_F - M_M)\exp(-B_M x) + M_M \tag{10}$$

Values for H_F and M_F were found by averaging the fibre indentation results across all locations, and were found to be $H_F = 5.44$ GPa and $M_F = 41.9$ GPa. Values for H_M and M_M are discussed in Section 3.2.3, and were found by averaging the matrix indentation results of each individual location after they stabilised into a plateau. For example, in Fig. 10a and b, this would be after $\times \approx 1.75$ μm and $\times \approx 2$ μm respectively.

A one-way ANOVA test was used to evaluate whether there was a significant difference in H_M and M_M results across the different tested locations (across the thickness of samples and across the same location of different samples), with a probability threshold value $\alpha = 0.05$. Whenever a significant difference is found, a one-way ANOVA test does not highlight which groups differ specifically. Therefore, when this happened, different result sets were tested together, and a T-test was performed whenever necessary to evaluate exactly which groups had a significant difference. This analysis can be found in the supplementary document.

Once these values were established, a MATLAB script was used to fit Eq. (9) and (10) to the raw data and find B_H (for hardness) and B_M (for elastic modulus) at each location □. These constants represent the gradient of the exponential decay function – the larger the value, the faster the transition from fibre to matrix hardness (or elastic modulus).

3.2.3. Matrix bulk properties (H_M and M_M)

In this section, a general comparison between compression-moulding and ATP results is drawn, followed by discussions within individual manufacturing processes (compression-moulded, ATP with T_{nip} 380 °C and ATP with T_{nip} 360 °C) addressed separately.

Note that ATP laminates with different nip temperatures are manufactured on different types of tools ($T_{nip} = 360$ °C on a ceramic tool and $T_{nip} = 380$ °C on a mild steel tool). This likely resulted in different cooling profiles in the laminates due to the different thermal conductivity of the tools. Therefore, results are not directly comparable.

Compression-moulded vs. ATP-380 laminates

The graphs in Fig. 11a and b show matrix bulk hardness and elastic modulus results for the compression-moulded laminates (single location tested as shown in Fig. 6b) and across the thickness of the ATP laminates with $T_{nip} = 380$ °C (3 locations tested as shown in Fig. 6c). These show that the compression-moulded laminates have significantly higher hardness (34–53 %) and elastic modulus (22–48 %) values than the ATP laminates (see supplementary document Section S.4). This is expected due to the extended holding times at crystallisation temperatures during manufacturing resulting in a crystalline matrix, whereas ATP laminates experienced fast-cooling, resulting in a softer, amorphous structure and lower hardness and elastic modulus responses.

Differences in compression-moulded laminates

Among the compression-moulded laminates, CM-260 performed marginally better (~9% higher hardness and 8–11 % higher elastic modulus), even though this difference was found not statistically significant (see supplementary document Section S.1). CM-220 and CM-300 performed similarly, as observed in Fig. 11. Previous work [7] performed on the same CF/PEKK prepreg tape showed that laminate CM-260 exhibited the fastest crystallisation rates. CM-220 and CM-300 possessed the smallest (~2 μm diameter) and largest (~6 μm) spherulites respectively (with CM-260 having intermediate-sized spherulites, ~4 μm). The faster crystallisation rates that CM-260 experienced might be an indication that these processing conditions are optimal for the polymer's most effective crystallisation, which has been reflected in its performance during nanoindentation testing.

On the other hand, mechanical properties of these samples reported in previous work (ILSS, 0° and 90° flexural [8]) did not show any significant effect of the spherulitic size. Tensile testing on other polymers with similar spherulite sizes (unreinforced PP-PE, 3–7 μm diameter) [43] reported similar findings. Polymers with larger variations in spherulitic diameter (1–30 μm), however, have shown a variation in mechanical performance (tensile and flexural), with unreinforced PA66 achieving a higher flexural modulus and yield point and a lower ultimate elongation with smaller spherulites [44]. Therefore, it might be

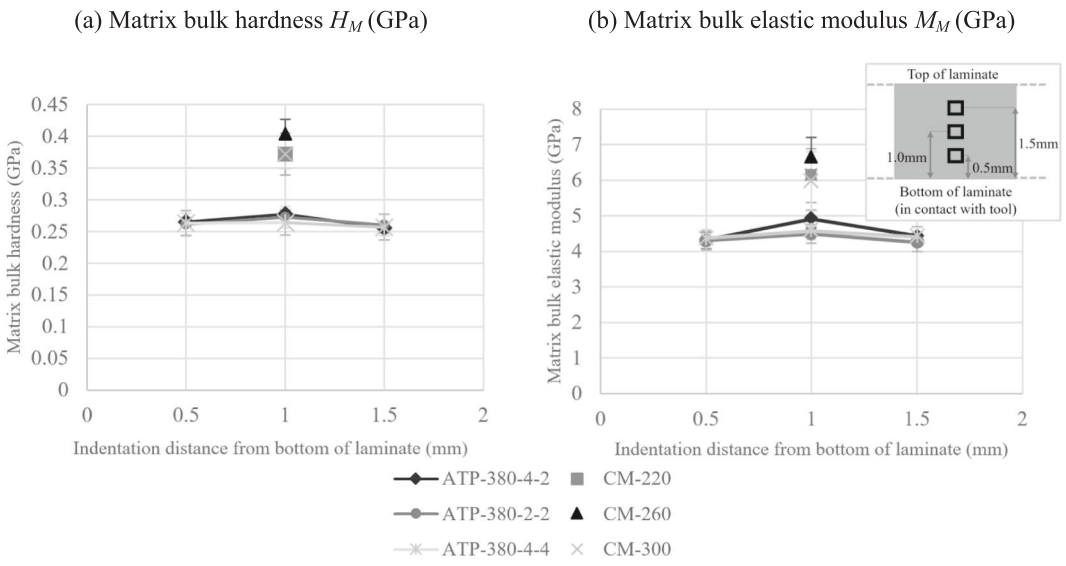

Fig. 11. (a) Matrix bulk hardness and (b) matrix bulk elastic modulus of all compression-moulded laminates and ATP laminates manufactured at $T_{nip} = 380$ °C. Top-right schematic shows the locations where the indentations were performed, measured from the bottom of the laminate (taken from Fig. 6).

possible that small variations in spherulite size may not have a significant impact on all mechanical properties at the macro scale, but their effects are more detectable at micron or nano-scale. The knowledge and understanding of such microstructures can improve the performance and failure at macroscopic level during the service life.

Differences in ATP-380 laminates (metal tool)

The results of all the ATP laminates (2 mm thick) shown in Fig. 11 follow a similar trend: a peak in properties in the middle of the laminate compared to the tested locations close to the bottom (tool side) and top surfaces. Percentage differences between the performance of the middle location and the top/bottom locations in the ATP laminates are as follows:

- ATP-380–4-2: 5–9 % hardness increase, 11–14 % elastic modulus increase.
- ATP-380–2-2: ~5% hardness increase, 4–5 % elastic modulus increase.
- ATP-380–4-4: 0–3 % hardness increase, 4–5 % elastic modulus increase.

This is likely due to the presence of two competing mechanisms during ATP manufacturing that influence crystallinity and mechanical properties:

- Proximity to the metal tool: the tool surface acts as a heat sink, contributing towards the fast cooling of the prepreg tape laid on it. As more layers of the laminate are laid, there is more material between the new prepreg layers and the tool. This can result in better heat retention and a reduction in the cooling speed, which contributes to crystallinity development. This has been observed for CF/PEEK [17], where prepreg layer crystallinity was found to be higher the further away the layer was from the bottom of the laminate (which was in contact with the tool surface), eventually plateauing to the maximum achievable crystallinity given the heat retention capability of the material and the ATP parameters. Ref. [17] also showed similar results on CF/PEKK, however, due to slower crystallisation kinetics, maximum achievable crystallinity was reached at a higher number of layers. The contribution of the proximity to the tool to crystallinity development is represented in Fig. 12 with a grey line, which resembles the results reported in [17] for the crystallinity evolution for every added layer.
- Heat repasses: as the prepreg layers are laid, the incoming heat diffuses into the layers that are already in place. This causes annealing of the polymer, which contributes towards enhanced crystallisation. The lower layers of the laminate undergo more of these repasses than the top layers. The through-thickness temperature profile of ATP-manufactured CF/PEEK laminates has been validated via

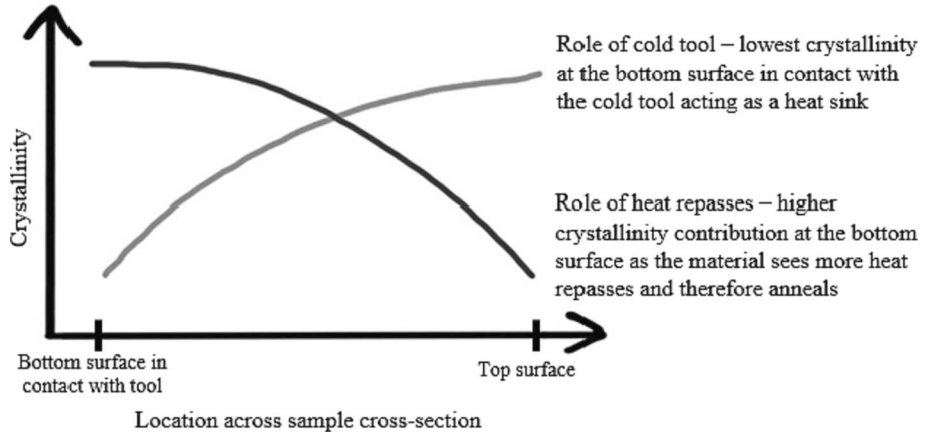

Fig. 12. Schematic of contribution to crystallinity development of the ATP unheated tool acting as a heat sink and the heat repasses seen by a layer of material as more layers are placed on top.

thermocouples during manufacturing [15,18,19] and modelled [15,18,20] in literature. The published literature shows that already laid material is repeatedly heated as more layers are placed. The contribution of heat repasses to crystallinity development is represented in Fig. 12 with a black line.

The optimal combination of these two competing mechanisms for the highest achievable crystallinity development may be reached around the middle layers of the laminate. The contribution of each mechanism is likely to change along with manufacturing parameters and the type of tool.

The difference in hardness and elastic modulus between ATP-380-4-2, ATP-380-2-2 and ATP-380-4-4 at the top and bottom locations is negligible and showed no statistically significant differences (see supplementary document Section S.2). This is likely due to the proximity to the tool on the bottom surface and the low number of (if any) repasses experienced by the top surface, where any variation in manufacturing parameters likely had a negligible effect on performance. It is therefore hypothesised that the fast-cooling and/or minimal annealing resulted in lower crystallinity compared to the middle location.

The middle location of the ATP-380-4-2 sample displayed a slightly higher hardness and elastic modulus than in the other two laminates, (2–5 % increase in hardness and 7–10 % in elastic modulus). The difference in elastic modulus particularly was statistically significant (supplementary document Section S.2).

Differences in ATP-360 laminates (ceramic tool)

The plots in Fig. 13 show matrix hardness and elastic modulus results for the compression-moulded laminates (single location tested as shown in Fig. 6b) and across the thickness of the 2 mm and 6 mm laminates with $T_{nip} = 360$ °C (3 locations tested as shown in Fig. 6c). The difference in performance between the compression-moulded laminates and the ATP-360 laminates (42–56 % hardness and 38–49 % elastic modulus) is similar to the ATP-380 laminates, for the same reasons as previously discussed, and is also statistically significant (see supplementary document Section S.5). Both ATP-360 laminates also displayed the same behaviour as the ATP-380 laminates, where the middle location of the laminates performed better than the top/bottom locations, with percentage differences as follows:

- 2 mm-thick laminate: 9–11 % hardness increase, 1–3 % elastic modulus increase.
- 6 mm thick laminate: 5–7 % hardness increase, 3–12 % elastic modulus increase.

This might be due to the central location having a higher crystallinity than the other tested locations, as described for the ATP-380 laminates. These differences were not statistically different (see supplementary document Section S.3).

3.2.4. Fibre/matrix interphase

As observed in Section 3.2.1, there is a fibre/matrix property transition in samples, whose response varies with the distance from the fibre surface. Section 3.2.2 introduced Eq. (9) and (10) to model this transition where B_H and B_M control the gradient of the fitted curves for hardness and elastic modulus data respectively. This section comments on any observed variations on these gradients across all compression-moulded laminates, as well as middle locations of ATP-380-4-2 and ATP-360-4-2-2 mm as representative ATP laminates to compare with the compression-moulding results.

Compression-moulded laminates

Table 3 provides B_H and B_M values and their 95 % confidence intervals for the compression-moulded laminates as calculated in

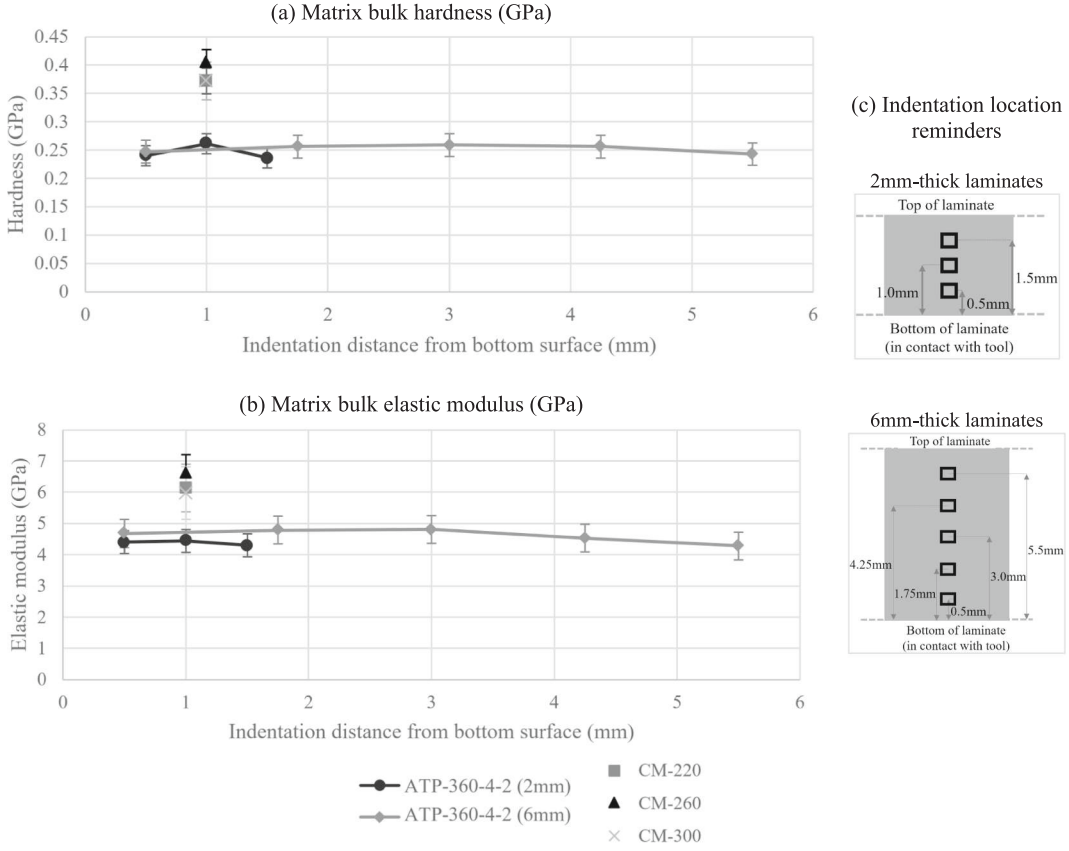

Fig. 13. (a) Matrix bulk hardness and (b) matrix bulk elastic modulus of all compression-moulded laminates and ATP laminates manufactured at $T_{nip} = 360$ °C. Schematics in (c) show the locations where the indentations were performed, measured from the bottom of the laminate (taken from Fig. 6).

Table 3
Summary of B_H and B_M values and 95% confidence intervals for the exponential decay modelling of compression-moulded CF/PEKK samples.

Laminate code	CM-220		CM-260		CM-300	
	Value	95 % confidence interval	Value	95 % confidence interval	Value	95 % confidence interval
B_H (Hardness)	1.918	±0.394	1.687	±0.344	1.924	±0.723
B_M (Elastic modulus)	1.421	±0.286	1.200	±0.197	1.411	±0.374

MATLAB. Fig. 14 shows the fitted exponential decay curves with the confidence intervals applied to the curves with shaded regions.

While gradient differences are subtle and all confidence intervals overlap with the plotted curves, these show that CM-260 is the laminate with the lowest B_H and B_M (the softest gradients), implying that this sample might have a slightly larger interphase than the other compression-moulded samples. This phenomenon could be explained with general polymeric nucleation theory, along with previous observations made on spherulite sizes of CF/PEKK at the temperatures used for compression moulding in this work. Fig. 15 has been included to aid with the explanation that follows.

- At lower crystallisation temperatures (the holding isothermal temperature at which the material is allowed to crystallise), primary nucleation dominates and there is minimal secondary nucleation. This means there will be a higher number of small spherulites, as shown in Fig. 15a. This is likely to also contribute towards the establishment of crystal nuclei (primary nucleation) on the fibre surface, but crystal growth as a consequence of secondary nucleation will be minimal. This might also result in a transcrystalline region at the fibre/matrix interface where any lamellar growth from the fibre is potentially very short and perpendicular to the fibre surface. This is likely the case for CM-220, as reported in our previous work [7] where SEM imaging of cryofractured CF/PEKK prepreg samples isothermally crystallised at 220 °C showed the formation of small spherulites, with some growth perpendicular to the fibre surface.
- At higher crystallisation temperatures, on the other hand, secondary nucleation dominates, resulting in a lower number of spherulites, but larger in size, as shown in Fig. 15c. This results in minimal primary nucleation taking place at the fibre surface, and so any crystals growing from the fibre surface will likely resemble spherulites from the bulk. It is therefore unlikely for there to be a significant interphase present. This is likely to be the case for CM-300, also shown in our previous work [7], where large spherulitic structures were observed on CF/PEKK samples isothermally crystallised at 300 °C.
- At the mid-range of crystallisation temperatures, however, there is a balance of both nucleation mechanisms, resulting in medium-sized spherulites. This might also allow for some primary nucleation to take place at the fibre surfaces but also for these nucleation sites to undergo secondary nucleation and develop a crystal structure/transcrystalline interphase between the fibre and the matrix. This is shown in Fig. 15b, and is likely representative of CM-260. CF/PEKK prepreg tape isothermally crystallised at 260 °C was observed to develop spherulites of intermediate size and perpendicular crystal growth from fibre surfaces, as reported in our previous work [7].

Compression-moulded vs. ATP laminates

Table 4 provides B_H and B_M values and their 95 % confidence intervals for CM-260, ATP-380-4-2 and ATP-360-4-2-2 mm as example laminates that underwent compression moulding, ATP with T_{nip} = 380 °C (with a metallic tool) and T_{nip} = 360 °C (with a ceramic tool). Fig. 16 shows the fitted exponential decay curves for each of these laminates, with their corresponding 95 % confidence intervals indicated by the shaded regions. CM-260 properties can be observed to plateau at a slightly higher value than the ATP laminates. This is due to the higher matrix bulk properties that compression-moulded samples possess, as discussed in Section 3.2.3.

In the case of the ATP laminates, the fast nature of the manufacturing is not ideal for developing a crystalline structure, as determined by the DSC results in Table 2. This is also the case for any fibre–matrix interphase formation. Even in the event of polymer melting during heating, the cooling rates that the material undergoes are too fast for any significant crystallinity to form in this grade of CF/PEKK [7]. Any further

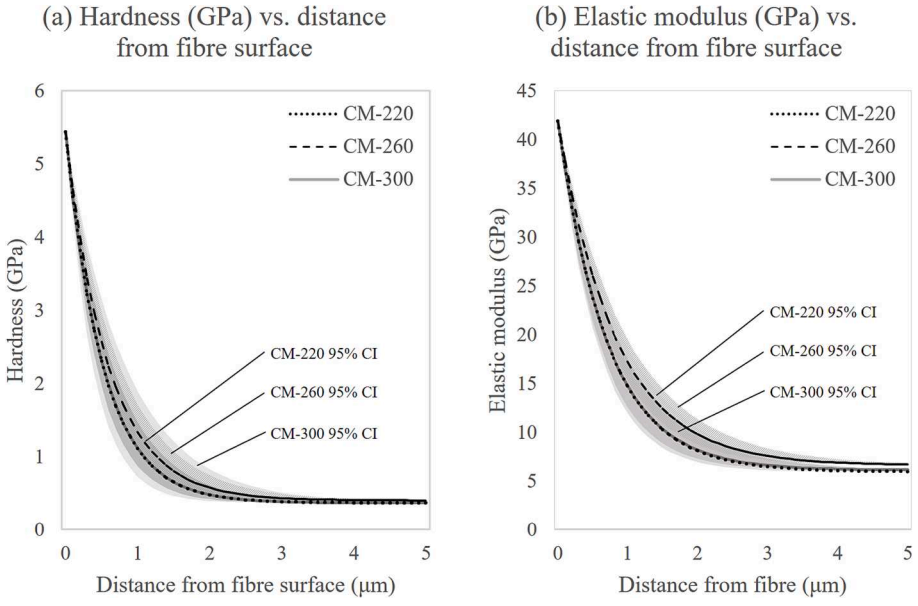

Fig. 14. (a) Hardness and (b) elastic modulus exponential decay curve fittings to nanoindentation test results of compression moulded samples, with 95% confidence intervals shown by the shaded regions. Note that the curves for CM-220 and CM-300 overlap in both plots.

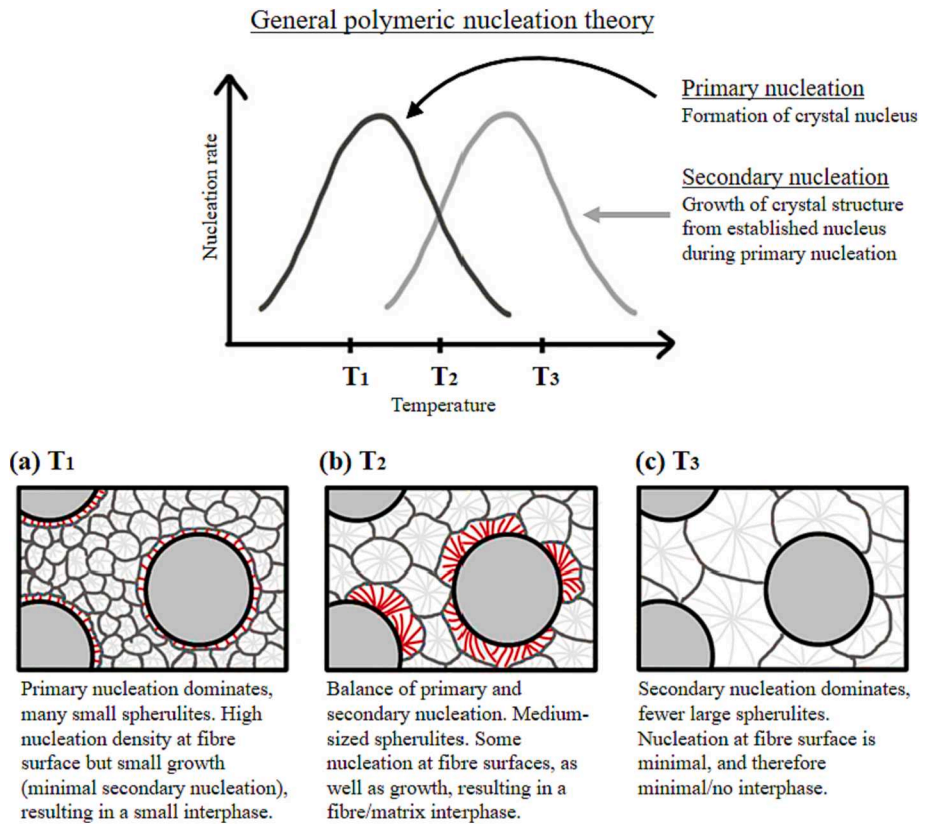

Fig. 15. Schematic demonstrating the effect of temperature on crystal growth in CF/PEKK, based on general polymeric nucleation theory, where $T_1 < T_2 < T_3$.

Table 4
Summary of B_H and B_M values and 95 % confidence intervals for the exponential decay modelling of CM-260, ATP-380-4-2 and ATP-360-4-2–2 mm.

Laminate code	CM-260		ATP-380–4-2 (MID)		ATP-360-4-2-2 mm (MID)	
	Value	95 % confidence interval	Value	95 % confidence interval	Value	95 % confidence interval
B_H (Hardness)	1.687	±0.344	3.816	±0.592	3.096	±0.885
B_M (Elastic modulus)	1.200	±0.197	1.687	±0.191	0.985	±0.211

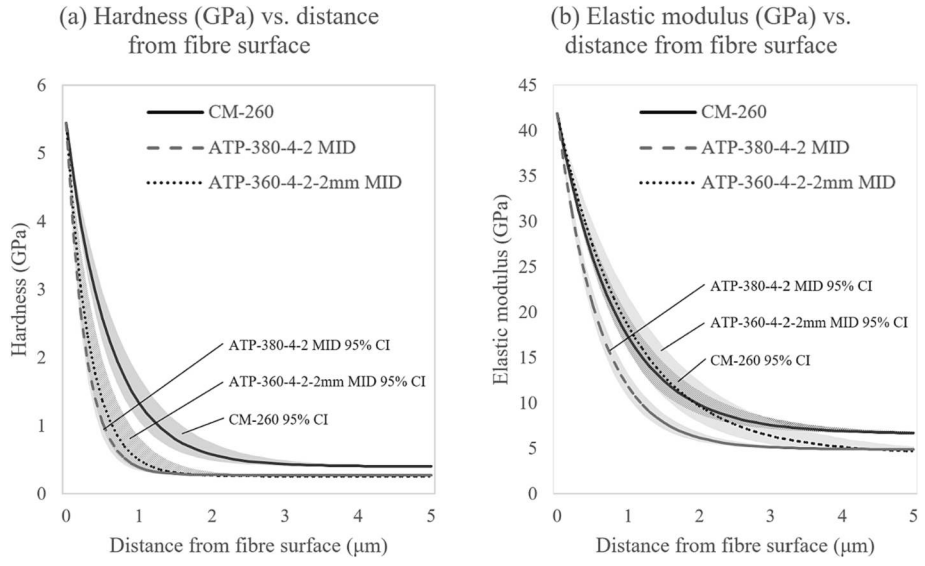

Fig. 16. (a) Hardness and (b) elastic modulus exponential decay curve fittings to nanoindentation test results of CM-260, ATP-380-4-2 and ATP-360-4-2-2 mm, with confidence intervals shown by the shaded regions.

crystallinity content developed during heat repasses is likely to take place at a smaller scale in the matrix bulk rather than at the interphase, due to molecular movement being considerably more restricted during annealing than during melt crystallisation. Therefore, any major rearrangement forming an interphase is unlikely.

The effect of overall crystallinity achieved is clearly reflected in the hardness results shown in Fig. 16a. Hardness is dictated by the load applied as per Eq. (4), and is more influenced by surface properties. Both ATP laminates possess a similar hardness response in the fibre/matrix transition region, whereas the compression-moulded laminate (with much higher crystallinity) shows a distinctly longer transition from fibre to matrix properties. This behaviour is not as obvious in Fig. 16b, where CM-260 and ATP-360-4-2-2 mm follow a similar transition path for the first micron from the fibre surface, after which CM-260 plateaus first to a higher value. The elastic modulus is influenced by the stiffness of the sample, as shown in Eq. (3), which is more interlinked with matrix bulk properties rather than surface properties as is the case of hardness. The marginally enhanced fibre–matrix transition behaviour in ATP-360 laminate might be attributed to the enhanced heat retention with the ceramic tool.

4. Conclusions

In this work, a series of CF/PEKK laminates were manufactured under a variety of compression-moulding and ATP conditions. DSC was carried out with each laminate in order to determine the crystallinity level achieved in each case. Nanoindentation experiments were performed that measured the hardness and elastic modulus of the samples reflecting their microstructural differences. A significant difference was observed in the performance of the matrix bulk across the different manufacturing techniques and conditions. A distinct variation in properties of the matrix bulk across the thickness of the ATP laminates was evident, for both 2 mm and 6 mm thickness, showing the presence of a crystallinity gradient. The presence of a fibre–matrix interphase and its variation under different processing conditions was also observed.

The matrix bulk of the compression-moulded laminates performed better than that of the ATP laminates by 34–53 % in hardness and 22–48 % in elastic modulus. This is expected, due to the higher crystallinity content of the compression-moulded laminates as a consequence of the longer holding times at crystallisation temperatures. CM-260, which had been observed to possess the fastest crystallisation rates in our previous work [7], performed the best among all the compression-moulded laminates by 9 % in hardness and 8–11 % in elastic modulus.

Variation in hardness and elastic modulus across the thickness of the ATP laminates was observed, with these properties being the highest in the middle of the laminate in all instances. This was likely due to the central region of the laminate cross-section achieving higher crystallinity, due to a combined effect of heat repasses from the added layers of material on top, and heat retention of the already laid material, allowing this middle section to hold heat for longer undergoing annealing.

Declaration of Competing Interest

The authors declare that they have no known competing financial interests or personal relationships that could have appeared to influence the work reported in this paper.

Data availability

Data will be made available on request.

Acknowledgements

The authors acknowledge the financial support received from the National Manufacturing Institute for Scotland (NMIS-IDP/009) and Hexcel Composites Limited.

The authors also wish to acknowledge the support of the Henry Royce Institute for Ms Helena Pérez-Martín through the Royce PhD Equipment Access Scheme, enabling access to nanoindentation facilities at the Materials Research Facility (UK Atomic Energy Authority).

Appendix A. Supplementary data

Supplementary data to this article can be found online at https://doi.org/10.1016/j.matdes.2023.112359.

References

[1] F. Rodríguez-Lence, M. Zuazo, S. Calvo, In-situ consolidation of PEEK composites by automated placement technologies, 20th Int. Conf. Compos. Mater. (2015) 19–24.
[2] J.P. Kilroy, C.M. Ó Brádaigh, C.O.A. Semprimoschnig, Mechanical and physical evaluation of a new carbon fibre/PEEK composite system for space applications, SAMPE J. (2008) 1–12.
[3] H. Pérez-Martín, P. Mackenzie, A. Baidak, C.M. Ó Brádaigh, D. Ray, Crystallinity studies of PEKK and carbon fibre/PEKK composites: A review, Compos. B Eng. 223 (2021) 109127.
[4] L. Quiroga Cortés, N. Caussé, E. Dantras, A. Lonjon, C. Lacabanne, Morphology and dynamical mechanical properties of poly ether ketone ketone (PEKK) with meta phenyl links, J. Appl. Polym. Sci. 133 (2016) 1–10, https://doi.org/10.1002/app.43396.
[5] T. Choupin, B. Fayolle, G. Régnier, C. Paris, J. Cinquin, B. Brulé, Isothermal crystallization kinetic modeling of poly(etherketoneketone) (PEKK) copolymer, Polymer 111 (2017) 73–82, https://doi.org/10.1016/j.polymer.2017.01.033.
[6] T. Choupin, B. Fayolle, G. Régnier, C. Paris, J. Cinquin, B. Brulé, A more reliable DSC-based methodology to study crystallization kinetics: application to poly(ether ketone ketone) (PEKK) copolymers, Polymer 155 (2018) 109–115, https://doi.org/10.1016/j.polymer.2018.08.060.
[7] H. Pérez-Martín, P. Mackenzie, A. Baidak, C.M. Ó Brádaigh, D. Ray, Crystallisation behaviour and morphological studies of PEKK and carbon fibre/PEKK composites, Compos. Part Appl. Sci. Manuf. 159 (2022) 106992.
[8] H. Pérez-Martín, S. Buchalik-Bopp, B.E. Guettler, P. Mackenzie, A. Baidak, C.M. Ó Brádaigh, et al., Effect of crystallinity and morphology on the mechanical properties of CF/PEKK composites manufactured under compression moulding and Automated Tape Placement, Mater. Today Commun. 36 (2023), https://doi.org/10.1016/j.mtcomm.2023.106442.
[9] S. Risteska, A.T. Petkoska, S. Samak, M. Drienovsky, Annealing effects on the crystallinity of carbon fiber-reinforced polyetheretherketone and polyohenylene laminate composites manufactured by laser automatic tape placement, Mater. Sci. 26 (2020) 308–316, https://doi.org/10.5755/j01.ms.26.3.21489.
[10] C.M. Stokes-Griffin, P. Compston, The effect of processing temperature and placement rate on the short beam strength of carbon fibre-PEEK manufactured using a laser tape placement process, Compos. Part Appl. Sci. Manuf. 78 (2015) 274–283, https://doi.org/10.1016/j.compositesa.2015.08.008.
[11] D. Saenz-Castillo, M.I. Martín, S. Calvo, F. Rodriguez-Lence, A. Güemes, Effect of processing parameters and void content on mechanical properties and NDI of thermoplastic composites, Compos. Part Appl. Sci. Manuf. 121 (2019) 308–320.
[12] A. Chanteli, A.K. Bandaru, D. Peeters, R.M. O'Higgins, P.M. Weaver, Influence of repass treatment on carbon fibre-reinforced PEEK composites manufactured using laser-assisted automatic tape placement, Compos. Struct. 248 (2020), 112539, https://doi.org/10.1016/j.compstruct.2020.112539.
[13] V.-T. Hoang, B.-S. Kwon, J.-W. Sung, H.-S. Choe, S.-W. Oh, S.-M. Lee, J.-H. Kweon, Y.-W. Nam, Postprocessing method-induced mechanical properties of carbon fiber-reinforced thermoplastic composites, J. Thermoplast. Compos. Mater. 36 (1) (2023) 432–447.
[14] A.J. Comer, D. Ray, W.O. Obande, D. Jones, J. Lyons, I. Rosca, R.M. O' Higgins, M. A. McCarthy, Mechanical characterisation of carbon fibre–PEEK manufactured by laser-assisted automated-tape-placement and autoclave, Compos. Part Appl. Sci. Manuf. 69 (2015) 10–20.
[15] M.B. Gruber, I.Z. Lockwood, T.L. Dolan, S.B. Funck, J.J. Tierney, P. Simacek, et al., Thermoplastic in situ placement requires better impregnated tapes and tows, Int. SAMPE Tech. Conf. (2012).
[16] G. Clancy, D. Peeters, V. Oliveri, D. Jones, R.M. O'Higgins, P.M. Weaver, A study of the influence of processing parameters on steering of carbon fibre/PEEK tapes using laser-assisted tape placement, Compos. B Eng. 163 (2019) 243–251, https://doi.org/10.1016/j.compositesb.2018.11.033.
[17] I. Esguerra-Arce, M.I. Martín, A. Pérez-Pastor, V. García-Martínez, Evolution of crystallinity with multiple lamination steps in high performance thermoplastic composites by in-situ consolidation process, Twenty-Second Int. Conf. Compos. Mater. (2019).
[18] A. Kollmannsberger, R. Lichtinger, F. Hohenester, C. Ebel, K. Drechsler, Numerical analysis of the temperature profile during the laser-assisted automated fiber placement of CFRP tapes with thermoplastic matrix, J. Thermoplast. Compos. Mater. 31 (2018) 1563–1586, https://doi.org/10.1177/0892705717738304.
[19] Lamontia MA, Gruber MB, Systems A, Drive S, Tierney J, Gillespie JW. Modeling the Accudyne Thermoplastic In Situ ATP Process. Proc SAMPE Conf 2009:8.

[20] J. Tierney, J.W. Gillespie, Modeling of heat transfer and void dynamics for the thermoplastic composite tow-placement process, J. Compos. Mater. 37 (19) (2003) 1745–1768.
[21] J.J. Tierney, J.W. Gillespie, Crystallization kinetics behavior of PEEK based composites exposed to high heating and cooling rates, Compos. Part Appl. Sci. Manuf. 35 (2004) 547–558, https://doi.org/10.1016/j.compositesa.2003.12.004.
[22] M.A. Lamontia, M.B. Gruber, Limitations on mechanical properties in thermoplastic laminates fabricated by two processes: automated thermoplastic tape placement and filament winding, SAMPE Eur. Conf. Exhib. (2005).
[23] C. Klapperich, K. Komvopoulos, L. Pruitt, Nanomechanical properties of polymers determined from nanoindentation experiments, J. Tribol. 123 (2000) 624–631, https://doi.org/10.1115/1.1330736.
[24] T. Iqbal, B.J. Briscoe, S. Yasin, P.F. Luckham, Nanoindentation response of poly (ether ether ketone) surfaces-A semicrystalline bimodal behavior, J. Appl. Polym. Sci. (2013), https://doi.org/10.1002/app.39723.
[25] P. Christöfl, C. Czibula, T. Seidlhofer, M. Berer, A. Macher, E. Helfer, T. Schrank, G. Oreski, C. Teichert, G. Pinter, Morphological characterization of semi-crystalline POM using nanoindentation, Int. J. Polym. Anal. Charact. 26 (8) (2021) 692–706.
[26] G.Z. Voyiadjis, A. Samadi-Dooki, L. Malekmotiei, Nanoindentation of high performance semicrystalline polymers: A case study on PEEK, Polym. Test. 61 (2017) 57–64, https://doi.org/10.1016/j.polymertesting.2017.05.005.
[27] B.R. Murray, A. Doyle, P.J. Feerick, C.O.A. Semprimoschnig, S.B. Leen, C.M. Ó Brádaigh, Rotational moulding of PEEK polymer liners with carbon fibre/PEEK over tape-placement for space cryogenic fuel tanks, Mater. Des. 132 (2017) 567–581, https://doi.org/10.1016/j.matdes.2017.07.026.
[28] D. Ray, A.J. Comer, J. Lyons, W. Obande, D. Jones, R.M.O. Higgins, M. A. McCarthy, Fracture toughness of carbon fiber/polyether ether ketone composites manufactured by autoclave and laser-assisted automated tape placement, J. Appl. Polym. Sci. (2014), https://doi.org/10.1002/app.41643.
[29] R.F. Gibson, A review of recent research on nanoindentation of polymer composites and their constituents, Compos. Sci. Technol. 105 (2014) 51–65, https://doi.org/10.1016/j.compscitech.2014.09.016.
[30] J.R. Gregory, S.M. Spearing, Nanoindentation of neat and in situ polymers in polymer–matrix composites, Compos. Sci. Technol. 65 (2005) 595–607, https://doi.org/10.1016/j.compscitech.2004.09.001.
[31] A. Molazemhosseini, H. Tourani, M.R. Naimi-Jamal, A. Khavandi, Nanoindentation and nanoscratching responses of PEEK based hybrid composites reinforced with short carbon fibers and nano-silica, Polym. Test. 32 (2013) 525–534, https://doi.org/10.1016/j.polymertesting.2013.02.001.
[32] A.K. Gain, E. Oromiehie, B.G. Prusty, Nanomechanical characterisation of CF-PEEK composites manufactured using automated fibre placement (AFP), Compos. Commun. 31 (2022), 101109, https://doi.org/10.1016/j.coco.2022.101109.
[33] E. Oromiehie, V. Nair, K. Short, T. Wei, D. Bhattacharyya, P.B. Gangadhara, Effect of He 2+ ion irradiation on the mechanical properties of automated fibre placement (Afp) Cf-peek thermoplastics, Composites (2023). https://doi.org/10.21203/rs.3.rs-3027646/v1.
[34] D. Gaitanelis, A. Chanteli, C. Worrall, P.M. Weaver, M. Kazilas, A multi-technique and multi-scale analysis of the thermal degradation of PEEK in laser heating, Polym. Degrad. Stab. 211 (2023), 110282, https://doi.org/10.1016/j.polymdegradstab.2023.110282.
[35] Y. Gaillard, F. Amiot, Grid nano-indentation as full-field measurements, Compos. Part Appl. Sci. Manuf. 132 (2020), 105807, https://doi.org/10.1016/j.compositesa.2020.105807.
[36] M. Hardiman, T.J. Vaughan, C.T. McCarthy, A review of key developments and pertinent issues in nanoindentation testing of fibre reinforced plastic microstructures, Compos. Struct. 180 (2017) 782–798, https://doi.org/10.1016/j.compstruct.2017.08.004.
[37] K. Ramaswamy, V. Modi, P.S. Rao, P.P. Martin, C.T. McCarthy, R.M. O'Higgins, An investigation of the influence of matrix properties and fibre–matrix interface behaviour on the mechanical performance of carbon fibre-reinforced PEKK and PEEK composites, Compos. A Appl. Sci. Manuf. 165 (2023) 107359.
[38] I.Y. Chang, B.S. Hsiao, Thermal properties of high performance thermoplastic composites based on poly(ether ketone ketone) (PEKK), in: 36th Int. SAMPE Symp., 1991, pp. 1587–1601.
[39] G.M. Pharr, W.C. Oliver, F.R. Brotzen, On the generality of the relationship among contact stiffness, contact area, and elastic modulus during indentation, J. Mater. Res. 7 (1992) 613–617, https://doi.org/10.1557/JMR.1992.0613.
[40] J.C. Hay, A. Bolshakov, G.M. Pharr, A critical examination of the fundamental relations used in the analysis of nanoindentation data, J. Mater. Res. 14 (1999) 2296–2305, https://doi.org/10.1557/JMR.1999.0306.
[41] W.C. Oliver, G.M. Pharr, An improved technique for determining hardness and elastic modulus using load and displacement sensing indentation experiments, J. Mater. Res. 7 (1992) 1564–1583, https://doi.org/10.1557/JMR.1992.1564.
[42] L. Shen, I.Y. Phang, T. Liu, Nanoindentation studies on polymorphism of nylon 6, Polym. Test. 25 (2006) 249–253, https://doi.org/10.1016/j.polymertesting.2005.09.019.
[43] J.C. Viana, A.M. Cunha, N. Billon, The effect of the skin thickness and spherulite size on the mechanical properties of injection mouldings, J. Mater. Sci. 36 (2001) 4411–4418.
[44] H.W. Starkweather, R.E. Brooks, Effect of spherulites on the mechanical properties of nylon 66, J. Appl. Polym. Sci. 1 (1959) 236–239, https://doi.org/10.1002/app.1959.070010214.